Materials Research. 2023; 26: e20230015
DOI: https://doi.org/10.1590/1980-5373-MR-2023-0015

Microstructural Characterization of a 1200 MPa Complex-Phase Steel

Renan de Melo Correia Lima[a], Julio Cesar Spadotto[a,b],

Flávia Tereza dos Santos Fernandes Tolomelli[c], Maria Isabel Ramos Navarro[a], Amy J. Clarke[d,e],

Kester D. Clarke[d,e,f], Fernando Cosme Rizzo Assunção[a]

[a]Pontifícia Universidade Católica do Rio de Janeiro (PUC-Rio), Departamento de Engenharia Química e de Materiais (DEQM), Rio de Janeiro, RJ, Brasil.
[b]Henry Royce Institute, Department of Materials, University of Manchester, Manchester, United Kingdom.
[c]Instituto Militar de Engenharia (IME), Departamento de Ciência e Engenharia de Materiais, Rio de Janeiro, RJ, Brasil.
[d]Colorado School of Mines, Center for Advanced Non-Ferrous Structural Alloys (CANFSA), Golden, CO, USA.
[e]Colorado School of Mines, Advanced Steel Processing and Products Research Center (ASPPRC), Golden, CO, USA.
[f]Colorado School of Mines, Forging Industry Educational and Research Fundation (FIERF), Golden, CO, USA.

Received: January 09, 2023; Revised: March 17, 2023; Accepted: April 13, 2023

The demand for new advanced high strength steels (AHSS) has been increasing in the last few decades. A large part of this demand comes from automotive companies. We have produced a new complex-phase (CP) steel with 1200 MPa of mechanical resistance and 8% of elongation, called CP1200. In this paper the dilatometric and microstructural characterization of a newly produced CP1200 steel is presented. The new steel was produced by making changes to the heat treatment of the already industrially available CP1100. The microstructure was quantified using light optical microscopy (LOM) and electron backscatter diffraction (EBSD). The microstructure of both steels was compared to identify the origin of the mechanical properties improvement. A new microstructure distribution, with higher amount of bainite and smaller concentration of ferrite and martensite was identified.

Keyword: *AHSS, Complex-Phase steel, Phase Transformation.*

1. Introduction

Complex-phase (CP) steels belong to a class of advanced high strength steels (AHSS) that has seen some increased use in the automotive industry in the past few years. Steels of this type have been used as substitutes for the more traditional Dual-Phase (DP) steels. The main difference between those classes is that CP steels present a higher yield strength and are less prone to void nucleation than DP steels, which makes the CP steels more workable with a higher stretch-flangeability. Both of these characteristics come from a higher amount of bainite in CP microstructures[1-9].

One important aspect, when working with CP steels, is to control their microstructure. Considerable variation in the mechanical properties can be achieved by manipulating heat treatment, making some industrially available steels even more competitive with small changes to their initial thermal treatment[10-14]. For this purpose, thermomechanical characterization using dilatometry or Gleeble simulations and microstructural characterization are widely applied to achieve improvements in the properties of AHSS.

However, the characterization of CP steels can be a challenge. Their microstructure may contain ferrite (intercritical and non-isothermal), bainite (including upper, lower, degenerated, granular and acicular), martensite, retained austenite and, in some cases, pearlite, making it hard to quantify without using several complementary characterization techniques. Therefore, combinations of light optical microscopy (LOM)[15] and electron backscatter diffraction (EBSD)[16-23] were used here for reliable quantification of microconstituent volume fractions.

Once both of those aspects are fulfilled (thermomechanical and microstructural characterization), a new heat treatment can be designed to optimize the mechanical properties. In this way, PUC-Rio and Companhia Siderúrgica Nacional (CSN) have been working in the development of a CP1200 steel that could be produced in an industrial scale to fulfill a commercial demand. Recently, a steel composition used to produce an industrial CP1100 steel had its continuing cooling transformation (CCT) diagram determined using dilatometry, and the microstructure analyzed using LOM and EBSD[14]. In the present work, a new heat treatment for this steel composition was designed using dilatometry and later reproduced in an industrial scale, resulting in a new CP1200 steel. The microstructure characterization of this newly produced steel is reported here.

*e-mail: renanmeloclima@gmail.com

2. Material

The chemical composition (% wt.) of the steel used in the present work contained 0.2Si, less than 0.17C, more than 1.6Mn, 0.015Al and 0.01Nb. The original CP1100 treatment yielded an average of 54 % ferrite, 21 % bainite, 19 % martensite and 2.5 % retained austenite measured by EBSD, LOM and X-ray diffraction[14].

The production of a CP steel can be largely divided in three steps: hot-rolling, cold-rolling, and heat treatment. The dilatometric results were obtained by treating cold-rolled steel samples extracted from the industrial processing of the CP1100 steel. The supplementary Figure S1 illustrates the sample origin in the industrial process. The cold rolled steel presented a ferritic/perlitic highly banded microstructure, with about 72 % of ferrite and 28 % of pearlite. The quantification was done using LOM and SEM imaging. The supplementary Figure S2, shows the typical microstructure of the steel.

Once the dilatometry results were obtained and the microstructural characterization was performed, a new heat treatment was designed and submitted to an industrial scale process. Samples of this process were used to measure the mechanical properties of the new steel.

3. Dilatometry

A DIL 805 from TA®instruments was used to perform controlled dilatometric heat treatments. Samples were machined using wire electrical discharge machining, and were 10 mm long, 4 mm wide and 1.4 mm thick. The derivative of the heating and cooling curves was used to ascertain the transformation temperatures.

Austenitization measurements were done by heating samples to temperatures between Ac_1 and Ac_3, holding for 5 min and then quenching to room temperature. Three soak temperatures were used in conjunction with the Ac_1 and Ac_3 to produce an austenitization curve by polynomial fitting in the OriginLab software.

4. Microstructural Characterization

Light optical microscopy (LOM) was conducted using an Olympus BX51M instrument. Samples were ground with silicon paper and polished using diamond suspensions. A color tint etching was performed initially using Nital to etch followed by $Na_2S_2O_5$ + water for tinting. This etching has been shown to reveal ferrite with whitish contrast, brown to dark brown martensite/bainite and black retained austenite in CP steels[15,16].

For EBSD, those sample were repolished in diamond suspensions up to 0.25 µm, followed by colloidal silica (MasterMet2®) polishing using an Minimet® and finishing using a 2 s etching in 0,5 % Nital.

A JEOL 7100 scanning electron microscope (SEM) was used to obtain secondary electron (SE) and backscattered electron (BSE) images. Microconstituents were identified by comparison with images from the literature[10,24].

Images were processed using the open-source software FIJI. The Waikato environment for knowledge analysis (WEKA)[25] plugin was used to train a neural network used for the phase segmentation of LOM and SEM images.

A Nordlys Max 2 detector and the X-Max 80 SDD were used for electron backscattered diffraction (EBSD) and X-ray energy dispersive spectroscopy (EDS), respectively. The EBSD maps were collected in 100x100 µm areas using a step size of 0,08 µm. The sample position required an IPF angles correction of (0°, -90°, 0). Regions for mapping were selected at $1/4$ of the thickness, avoiding both the edge and the center of the steel sheet.

In the EBSD results, retained austenite was identified by its crystal structure in the phase map. Martensite, due to its high deformation, appeared as zero solution in the phase identification and it was segmented as such. Ferrite and bainite were differentiated by taking in consideration that bainite is a deformed microconstituent, due to its higher dislocation density; therefore, by using the kernel average misorientation (KAM) and grain orientation spread (GOS) maps it was separated from the less deformed ferrite[14,16,17,19,26,27].

This segmentation process was performed using the AZtecCrystal software[28]. This software applies a machine learning process to identify the microconstituents based on the before mentioned maps.

5. Mechanical Properties

To measure the mechanical properties of the new industrially processed steel, tensile, bending and hole expansion tests were conducted at CSN production line. An Instron 5585H 25 t instrument with an AVE extensometer and sub dimensioned 50 mm tensile samples following the ASTM E8[29] norm were used for tensile testing. The bending tests were done following the ASTM E290[30] using a vise and a bend supporter with 3.5 times the plate thickness. The bending was first done to 90º for the regular test, and then extended until damage was perceived. The hole expansion test was done following the standard ISO-TS 16630[31] and using a homemade device.

Hardness measurements were done using a Wolpert Wilson Instruments™ universal hardness tester closed loop 930N. The testing was done following the ASTM E92 – 17 standard[32] "standard test methods for Vickers hardness and Knoop hardness of metallic materials".

6. Results

The dilatometric change in length versus temperature curve, resulting from the heat treatment applied in the present work is shown in Figure 1. The heating rate is slowed near the holding temperature to guarantee a more homogeneous heating. This, combined with the austenitization contraction, produces the odd behavior observed during austenite formation. As soon as cooling begins, intercritical ferrite starts to grow and, at the same time, some new ferrite grains will be formed. The fast cooling makes hard to see the change in length caused by the ferrite growth and formation, but in Figure S3 a zoomed segment of the dilatometry curve shows the start and finish of the nucleation of new ferrite grains (the zoomed region is marked in Figure 1). Also in Figure 1, a large non-isothermal bainite transformation can be seen, followed by an isothermal bainite formation.

An industrial scale reproduction of the treatment was conducted to investigate the mechanical properties. The results of the tensile and hardness testing and its comparison to the CP1100 can be seen in Table 1.

The bending test showed satisfactory results, with no cracking in 90º bending. Further testing showed small signs of crack formation above 105º of bending. A λ value of 120 % was obtained in the hole expansion testing.

An austenitization curve was produced by applying a polynomial fitting in the austenite content of the Ac_1, Ac_3 as well as samples heated and held for 5 min at three temperatures between Ac_1, Ac_3 followed by quenching using a 50° C/s rate. The ferrite was quantified in those samples and used as a measure of the austenitization; the continuous cooling transformation curve for this composition shows that this cooling rate prevents ferrite formation[14]. Figure 2 shows the resulting austenitization curve. Figure S4 shows the microstructure (Nital etched) from two of the samples used in this process.

Figure 3 presents a LOM image of the treated steel and its segmentation. In Figure 3A whitish regions are ferrite, brown regions are martensite/bainite, and black regions are retained austenite. In Figure 3B the LOM was segmented with red ferrite, green martensite/bainite and magenta retained austenite.

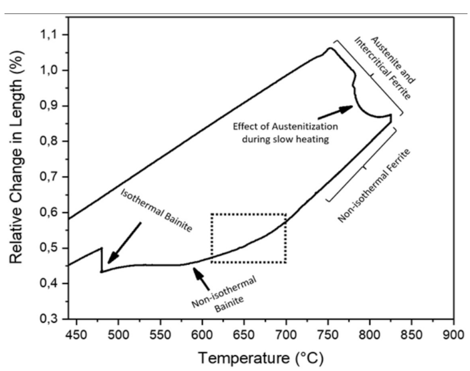

Figure 1. Change in length by temperature result of the new heat treatment. Selected area is shown in higher magnification in Figure S3.

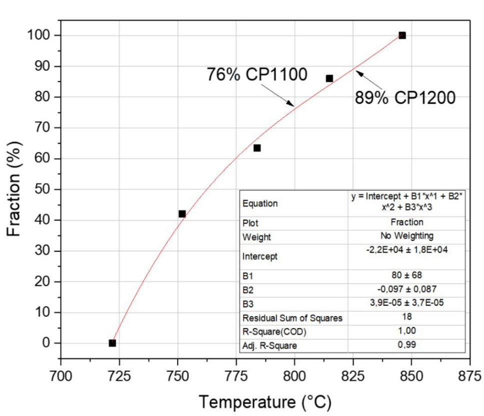

Figure 2. Austenitization curve for the steel composition.

Comparing the microstructure from the material studied in the present work to the prior CP1100[14], the former presents less ferrite and more bainite/martensite than the CP1100. The LOM images were segmented using WEKA plugin, the result of the segmentation and its comparison to the CP1100 are summarized in Table 2. The table was obtained using 9 LOM images in 500x magnification for a total area of about 0,01 cm^2.

Figure 4 presents SEM images of the steel subjected to new treatment. The steel preserves a small remnant orientation in the rolling direction, seen by its banded behavior primarily in small magnifications. In Figure 4B, green arrows point to the ferritic regions and black arrows to martensite/austenite islands. It is difficult to properly identify bainite in the SEM image, so EBSD analysis was used for that purpose.

Figure 5 shows an example of a segmented EBSD map and the steps that lead to it. Figure 5A shows the Band Contrast (BC). Figure 5B shows the Inverse Pole Figure (IPF). The steel presents a (111) preferential orientation, which was also observed in the CP1100 counterpart. Figure 5C shows the combination of BC, KAM and GOS maps. Figure 5D shows the final segmentation and the insert in the figure highlight the small, retained austenite grains. The segmentation was done using Aztec Crystal software. A total of eleven regions were used for the collection of the EBSD maps in order to have a more representative result; the average microconstituent distribution, and its comparison to the CP1100[14] is presented in Table 3.

7. Discussion

The steel produced using the new heat treatment results in properties that meet the requirements of a CP1200 classification,

Table 1. Tensile and Hardness proprieties of the CP1100 and its comparison to the new treatment.

Steel	YS(MPa)	UTS(MPa)	El. (%)	HV10
CP1100	831	1112	9	324
New Treatment	820	1278	10.5	337

Table 2. Microconstituents quantification comparison from LOM images between the CP1100 and the new treatment.

Steel	Ferrite %	Bainite/ Martensite %	Retained Austenite%
CP1100	54 ± 3.7	45.3 ± 3.6	0.78 ± 0.25
New Treatment	47.4 ± 1.97	50.34 ± 1.64	0.4 ± 0.18

Table 3. EBSD quantification comparison between the CP1100 and the new treatment.

Steel	Ferrite %	Bainite %	Martensite %	RA %
CP1100	56.3 ± 4	21.1 ± 4.1	21.2 ± 1.5	1.4 ± 1
New Treatment	47 ± 4.4	35.8 ± 2	16.7 ± 3.9	0.4 ± 0.2

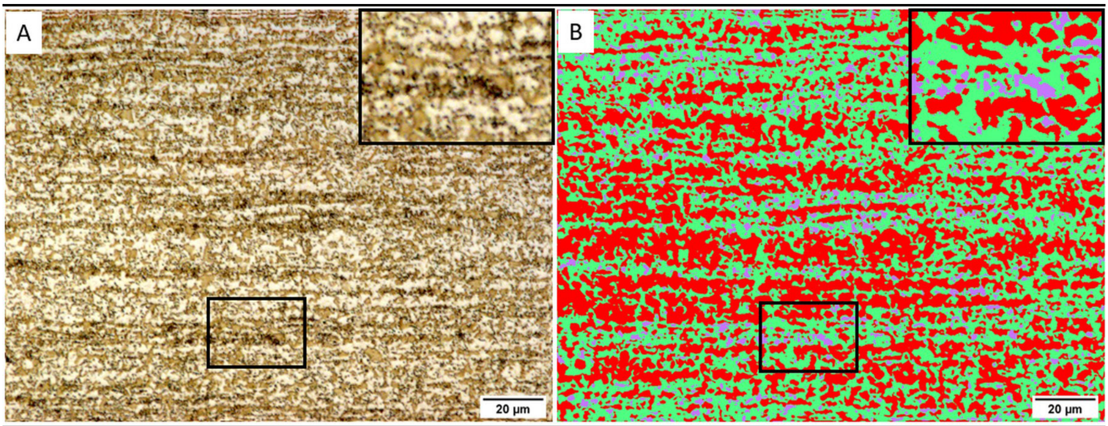

Figure 3. LOM and segmented images of the CP1200 etched using Nital /$Na_2S_2O_5$. A – Whitish ferrite, brown martensite/bainite, black retained austenite. B – Red ferrite, green bainite/martensite, magenta retained austenite. Insert in A and B shows a region of retained austenite.

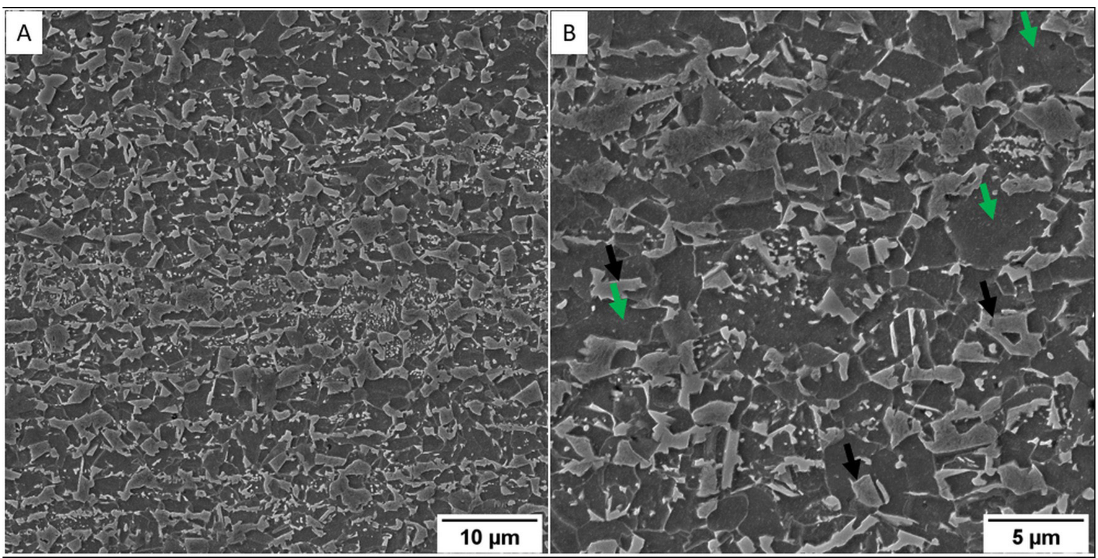

Figure 4. SEM image of the CP1200 etched using Nital /$Na_2S_2O_5$. A – Lower magnification image. B – Higher magnification image, black arrows point to M/A islands, green arrows point to ferrite.

including a 1200 MPa tensile strength, greater than 800 MPa yield strength and at least 8 % of total elongation.

Considering that the composition of the steel was the same of the CP1100[14], it can be stated that the improvement in the mechanical properties came directly from the new microstructural distribution. The LOM results had already presented a substantial decrease in ferrite content and the EBSD quantification further showed an increase of about 15 % in the bainite content, as shown in Table 3.

Prior results from other researchers[7,8,33] have shown that the presence of bainite in the microstructure can reduce or delay the void nucleation.

The increase in the amount of bainite with a corresponding delay in void nucleation can explain the 100 MPa increase in mechanical strength together with the small improvement (1.5 %) to the elongation. A more extensive study of the interface distribution and its influence in the mechanical properties is needed to better understand this aspect. The amount and distribution of interfaces such as ferrite-martensite, bainite-ferrite and bainite-martensite can be the key to understand and minimize the void nucleation.

The new treatment also resulted in a higher orientation in the (111) direction. This may be due to the formation of higher amounts of bainite as this microconstituent is known to grow in low energy boundaries[34]. Texture can be an important aspect for automotive steel. Many applications can be benefitted by a texture that resists stamp deformation. Research in the texture evolution from the hot rolling to the final product and its influence in the mechanical properties is being conducted.

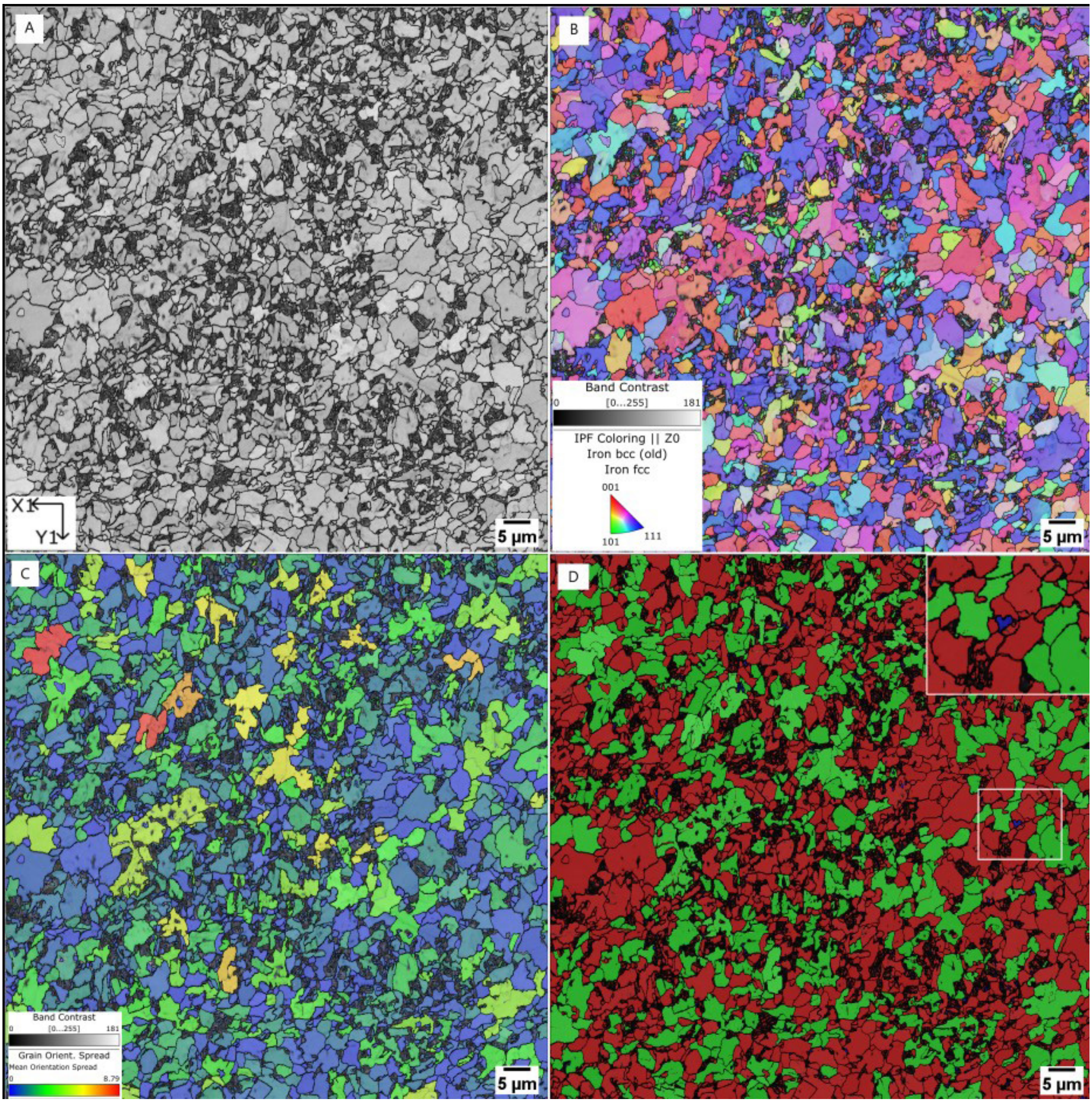

Figure 5. EBSD analysis maps. A – Band Contrast map. B – Band Contrast + Inverse Pole Figure maps. C – Band Contrast + Grain Orientation Spread maps, blue grains have low deformation, green and red have higher deformation. D – Segmented map, red ferrite, green bainite, black martensite and blue retained austenite. Inset in figure D shows a small austenite region.

8. Conclusions

A new heat treatment was designed and performed, first in a dilatometer and later at the industrial scale. The steel composition corresponded to an industrial CP1100. The new heat treatment produced a steel with improved mechanical properties that classified the new steel as a CP1200. LOM and EBSD characterization of the new steel showed an increase of about 15 % in the bainite content and a decrease in the ferrite (~10 %) and martensite (~5 %) contents when comparing to the CP1100 microstructure. This new microstructural distribution led to the mechanical property improvement. The improvement was attributed to the higher concentration of bainite that made the steel less prone to void nucleation. Further research in the interface distribution, texture evolution and its influence in the mechanical properties will be conducted.

9. Acknowledgements

The authors would like to acknowledge the institutions and funding agencies involved in this work: PUC-RIO; CSN; CANFSA and ASPPRC from MINES; LABNANO from Centro Brasileiro de Pesquisas Físicas (LABNANO-CBPF); Laboratório de Transformações de Fase from Universidade de São Paulo (LTF-USP); Instituto Nacional de Tecnologia (INT); Coordenação de Aperfeiçoamento de Pessoal de Nível Superior (CAPES); Conselho Nacional de Desenvolvimento Científico e Tecnológico (CNPq) and the Fundação Carlos Chagas Filho de Amparo a Pesquisa do Estado do Rio de Janeiro (FAPERJ).

10. References

1. Cornette D, Hourman T, Hudin O, Laurent JP, Reynaert A. High strength steels for automotive safety parts. SAE Tech Pap Ser. 2001;(724):1-14.

2. Mesplont C. Phase transformations and microstructure - mechanical properties relations in complex phase high strength steels. [thesis]. België: Universiteit Gent; 2002. [cited 2023 Jan 9]. Available from: https://core.ac.uk/download/pdf/55810853.pdf
3. Gutierrez I, Altuna A, Paul G, Parker SV, Bianchi JH, Vescovo P, et al. Mechanical property models for high-strength complex microstructures. Luxembourg: Office for Official Publ. of the E.U.; 2010.
4. Mallick PK. Advanced materials for automotive applications: an overview. In Rowe J, editor. Advanced materials in automotive engineering. Sawston, Reino Unido: Woodhead Publishing; 2012. p. 5-27.
5. Hilditch TB, de Souza T, Hodgson PD. Properties and automotive applications of advanced high-strength steels (AHSS). In: Shome M, Tumuluru M, editors. Welding and Joining of Advanced High Strength Steels (AHSS). Sawston, Reino Unido: Woodhead Publishing; 2015. p. 9-28. http://dx.doi.org/10.1016/B978-0-85709-436-0.00002-3.
6. Hall JN, Fekete JR. Steels for auto bodies: a general overview. In: Rana R, Singh SB, editors. Automotive steels: design, metallurgy, processing and applications. Sawston, Reino Unido: Woodhead Publishing; 2017. p. 19-45. http://dx.doi.org/10.1016/B978-0-08-100638-2.00002-X.
7. Pathak N, Butcher C, Worswick MJ, Bellhouse E, Gao J. Damage evolution in complex-phase and dual-phase steels during edge stretching. Materials (Basel). 2017;10(4):1-29.
8. Martin P, Unruh K, Chottin J, Hug E. Damage mechanisms in multiphased steels with a bainitic matrix under various mechanical loading paths. Procedia Manuf. 2018;15:1557-64. https://doi.org/10.1016/j.promfg.2018.07.317.
9. Horvath CD. Advanced steels for lightweight automotive structures. In: Mallick PK, editor. Materials, design and manufacturing for lightweight vehicles. Sawston, Reino Unido: Woodhead Publishing; 2021. p. 39-95. http://dx.doi.org/10.1016/B978-0-12-818712-8.00002-1.
10. Da Silva EF, Pereira DHM, Yadava YP, Araujo OO Fo, Sanguinetti Ferreira RA. Influence of thermomechanical sequences on the mechanical properties of dp 800 steel. Mater Res. 2021;24(3):2-8.
11. Caballero FG, Miller MK, Garcia-Mateo C, Capdevila C, Garcia de Andrés C. Phase transformation theory: a powerful tool for the design of advanced steels. JOM. 2008;60(12):16-21.
12. Tomita Y, Okabayashi K. Modified heat treatment for lower temperature improvement of the mechanical properties of two ultrahigh strength low alloy steels. Metall Trans, A, Phys Metall Mater Sci. 1985;16(1):83-91.
13. Hairer F, Krempaszky C, München U. Effects of heat treatment on microstructure and mechanical properties of bainitic single- and complex-phase steel. Mater Sci Technol. 2018;2009:1391-401.
14. Lima RMC, Tolomelli FTS, Clarke AJ, Clarke KD, Spadotto JC, Assunção FCR. Microstructural characterization of A 1100 MPa complex-phase steel. J Mater Res Technol. 2022;17:184-91.
15. Hairer F, Karelová A, Krempaszky C, Werner E, Pichler T, Hebesberger A. Etching techniques for the microstructural characterization of complex phase steels by light microscopy. Int Dr Semin [Internet]. 2008; [cited 2023 jan 9];50-4. Available from: http://www.mtf.stuba.sk/docs/internetovy_casopis/2008/4mimorc/hairer.pdf
16. Lima R MC, Spadotto J, Rizzo FC. Use of LOM and EBSD to identify bainite in complex phase steel. Microsc Microanal. 2021;27(S1):370-2.
17. Li X, Ramazani A, Prahl U, Bleck W. Quantification of complex-phase steel microstructure by using combined EBSD and EPMA measurements. Mater Charact. 2018;142:179-86. http://dx.doi.org/10.1016/j.matchar.2018.05.038.
18. Na S-H, Seol J-B, Jafari M, Park C-G. A correlative approach for identifying complex phases by electron backscatter diffraction and transmission electron microscopy. Appl Microsc. 2017;47(1):43-9.
19. Zhao H, Wynne BP, Palmiere EJ. A phase quantification method based on EBSD data for a continuously cooled microalloyed steel. Mater Charact. 2017;123:339-48. http://dx.doi.org/10.1016/j.matchar.2016.11.024.
20. Bleck W, Phiu-on K. Effects of microalloying in multi phase steels for car body manufacture. In: Haldar A, Suwas S, Bhattacharjee D, editors. Microstructure and texture in steels. London: Springer; 2009. p. 145-63.
21. Kang JY, Kim DH, Baik S-Il, Ahn TH, Kim YW, Han HN, et al. Phase analysis of steels by grain-averaged EBSD functions. ISIJ Int. 2011;51(1):130-6.
22. Oxford I. Rapid clasification of advanced high strength steels using EBSD [Internet]. Abingdon: Oxford Instruments; 2020 [cited 2023 jan 9]. Available from: https://nano.oxinst.com/assets/uploads/products/nanoanalysis/documents/Application Notes/AZtec QP Steels.pdf
23. Pinard PT, Schwedt A, Ramazani A, Prahl U, Richter S. Characterization of dual-phase steel microstructure by combined submicrometer EBSD and EPMA carbon measurements. Microsc Microanal. 2013;19(4):996-1006.
24. Santofimia MJ, Zhao L, Sietsma J. Microstructural evolution of a low-carbon steel during application of quenching and partitioning heat treatments after partial austenitization. Metall Mater Trans, A Phys Metall Mater Sci. 2009;40(1):46-57.
25. Arganda-Carreras I, Kaynig V, Rueden C, Eliceiri KW, Schindelin J, Cardona A, et al. Trainable weka segmentation: a machine learning tool for microscopy pixel classification. Bioinformatics. 2017;33(15):2424-6.
26. DeArdo AJ, Garcia CI, Cho K, Hua M. New method of characterizing and quantifying complex microstructures in steels. Mater Manuf Process. 2010; 25(1-3), p. 33-40. https://dx.doi.org/10.1080/10426910903143415.
27. Pinto LA, Pérez Escobar D, Santos OSH, Lopes NIA, Carneiro JRG, Ribeiro-Andrade R. Influence of surface preparation method on retained austenite quantification. Mater Today Commun. 2020;24:101226.
28. Oxford Instruments. AZtec® reclassify phase: discriminating phases in steels [Internet]. Abingdon: Oxford Instruments; 2016 [cited 2023 jan 9]. Available from: https://nano.oxinst.com/campaigns/downloads/aztec-reclassify-phase-discriminating-phases-in-steels
29. ASTM: American Society for Testing and Materials. ASTM E8/E8M-22: standard test methods for tension testing of metallic materials [Internet]. West Conshohocken: ASTM; 2022 [cited 2023 jan 9]. Available from: https://www.astm.org/e0008_e0008m-22.html
30. ASTM: American Society for Testing and Materials. ASTM E0290-14: standard test methods for bend testing of materials for ductility [Internet]. West Conshohocken: ASTM; 2022 [cited 2023 jan 9]. Available from: https://www.astm.org/e0290-14.html
31. ISO: International Organization for Standardization. ISO/TS 16630:2003: metallic materials -- Method of hole expanding test [Internet]. Geneva, Switzerland: ISO; 2003.
32. ASTM: American Society for Testing and Materials. ASTM E92-17: standard test methods for vickers hardness and knoop hardness of metallic materials [Internet]. West Conshohocken: ASTM; 2017 [cited 2023 jan 9]. Available from: https://www.astm.org/Standards/E92.htm
33. Karelova A, Krempaszky C, Werner E, Tsipouridis P, Hebesberger T, Pichler A. Hole expansion of dual-phase and complex-phase AHS steels - effect of edge conditions. Steel Res Int. 2009;80:71-7.
34. Cabus C, Réglé H, Bacroix B. Orientation relationship between austenite and bainite in a multiphased steel. Mater Charact. 2007;58(4):332-8.

Supplementary material

The following online material is available for this article:

Figure S1 - Schematic design of the Complex-Phase steel heat treatment. Green arrow point to were in the process the samples for heat treatment were taken.

Figure S2 - Typical microstructure of the steel in the cold rolled condition. A show a low magnification image with a highly banded microstructure. B – Presents a higher magnification image. The black arrow points to the perlite microconstituent, yellow arrow points to the ferrite.

Figure S3 - Zoom in in the CP1200 heat treatment cycle showing the ferrite start and ferrite end points.

Figure S4 - LOM image of the samples used in the austenitization curve. A – Sample held at about 750°C. B – samples held at 810°C. Whitish ferrite, brown martensite.